THE JOURNAL OF PHYSICAL CHEMISTRY Letters

Letter

pubs.acs.org/JPCL

Enhanced-Resolution Single-Shot 2DFT Spectroscopy by Spatial Spectral Interferometry

Austin P. Spencer, Boris Spokoyny, and Elad Harel*

Department of Chemistry, Northwestern University, 2145 Sheridan Road, Evanston, Illinois 60208, United States

ABSTRACT: We demonstrate use of spatial interference for the complete electric field reconstruction of two-dimensional (2D) coherent spectroscopic signals generated through four-wave mixing (4WM) in a single laser shot. Until now, the amplitude and phase characterization of 4WM signals has relied primarily on Fourier transform spectral interferometry (FTSI), which limits the measurement's sensitivity and resolution. We show that spatial spectral interferometry (SSI) is a generalized approach to 4WM signal detection that eliminates these inherent limitations of FTSI without introducing additional experimental complexity. SSI is used to measure the 2D photon echo spectra of two systems with dramatically different line widths, the coupled D line transitions in rubidium vapor and the energy-transfer dynamics in the light-harvesting protein LH2.

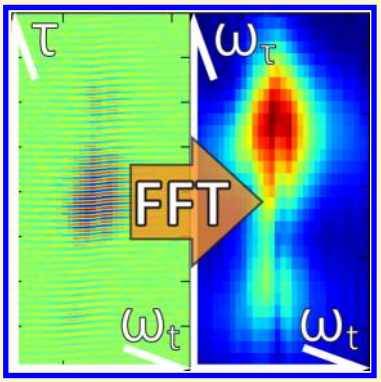

Two-dimensional Fourier transform spectroscopy[1−4] (2DFT) probes correlated optical transitions and femtosecond time scale dynamics in complex, condensed-phase molecular systems. Applications of two- and higher-dimensional coherent spectroscopic methods in the infrared,[5] visible,[3] and ultraviolet[6] spectral regions have been demonstrated for probing various photophysical properties in a wide range of materials and biological systems such as semiconductors,[7,8] atomic alkali vapors,[9,10] hydrogen-bonded networks,[11] and pigment−protein complexes.[12,13]

One main method for measuring 2DFT spectra is by acquiring the phase-matched signal radiated in a four-wave mixing (4WM) process. The advantages of this method include background-free measurements (in the case of a fully noncollinear phase-matched geometry) and reduced acquisition time when directly detecting the signal field in a spectrograph. GRadient-Assisted Photon Echo Spectroscopy (GRAPES),[12,14] an extension of the three-pulse photon echo (3PE) method for 2DFT spectroscopy, acquires a 2DFT spectrum in a single laser shot, greatly reducing the mechanical stability requirements and further minimizing the acquisition time compared to conventional delay-scanning approaches. GRAPES harnesses a spatial dimension of the excitation pulses to spatially encode temporal information in the sample, multiplexing what would otherwise be parametric sampling of pulse delay times. Here, we demonstrate the use of spatial interference (at the detector) in the 4WM signal detection alongside the inherent spatial interference (at the sample) that spatially encodes the signal in GRAPES. The introduction of spatial interference allows for higher resolution in spectral phase recovery and greater sensitivity compared to spectral interference alone.

Fourier transform spectral interferometry[15−20] (FTSI) is a well-developed method for measuring the spectrum and spectral phase of 4WM signals. FTSI relies on spectral interference between the signal field and a reference field (separated in time by several pulse durations), therefore requiring frequency resolution at the detector several times that needed to merely resolve the spectral features in the signal field.[21] Practically, this limits the frequency resolution of the recovered spectral phase to a fraction (typically about one-fifth) of the spectrometer resolution.[21] For signal fields with spectral widths on the order of the spectrometer resolution, FTSI will fail because the spectral fringe spacing necessary to isolate the interference peaks from low-frequency (DC) peaks in the Fourier transformed spectral interferogram will fall below the spectrometer resolution.

Spatial spectral interferometry (SSI) is an extension of spectral interferometry in which the signal and reference beams cross and overlap spatially at the detector such that spatial interference fringes are formed. This technique has been utilized[21,22] for pulse characterization, where it enables shot-to-shot recovery of the pulse spectrum and spectral phase with high frequency resolution. SSI does not require a time delay between signal and reference fields, although it can accommodate such a configuration. Fourier transforming along the spatial dimension enables the signal−reference interference terms to be isolated. Because the interference occurs along a spatial dimension orthogonal to the spectrally dispersed dimension, the full resolution of the spectrometer can be utilized in spectral phase recovery.[21] In addition, use of spatial interference fringes for signal isolation in SSI, as opposed to spectral fringes as in FTSI, reduces the required spectral resolution to only that necessary to resolve the signal spectrum.

Received: February 8, 2015
Accepted: February 25, 2015

DOI: 10.1021/acs.jpclett.5b00273
J. Phys. Chem. Lett. 2015, 6, 945−950

In this work, we demonstrate the application of SSI to GRAPES for detecting 4WM signals generated in rubidium (Rb) vapor and in LH2, a light-harvesting complex found in purple bacteria. These systems have transitions with widely different spectral widths, ranging from less than 1 cm^{-1} for the collisionally broadened rubidium vapor D lines to more than 300 cm^{-1} for the B800 and B850 bands in LH2, demonstrating the flexibility of SSI. Due to the exceptional narrowness of the Rb D lines, whose widths are on the order of our spectrometer resolution (~0.5 cm^{-1}), this experiment would not be possible with traditional FTSI.

Spatial interference (induced by a nonzero crossing angle between beams) can be used either on its own or in conjunction with spectral interference (induced by a nonzero time delay between fields). When used together, spatial interference compliments spectral interference by relaxing frequency resolution requirements and therefore increasing sensitivity. In principle, use of SSI instead of FTSI introduces no new experimental complexity to a GRAPES experiment because the signal−beam 4 crossing angle must be characterized in either case. Likewise, no additional calibration measurements are necessary for SSI compared to FTSI, although new methods for processing and utilizing these calibration measurements are presented here.

The theory of 2DFT spectroscopy has been described elsewhere,[3,4,23,24] and therefore, we will focus on the aspects related to GRAPES and signal recovery. In conventional 2DFT spectroscopy, the time delay τ between pulses 1 and 2 (Figure 1a.i) is sequentially scanned to build up a set of interferograms

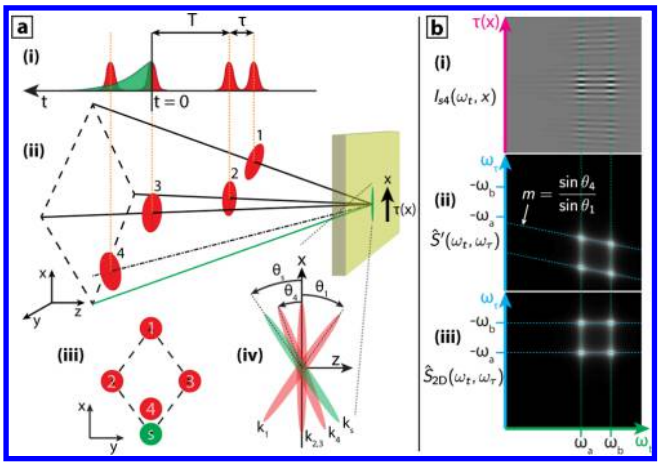

Figure 1. (a) Illustration of (a.i) the pulse sequence and (a.ii) the noncollinear phase-matching geometry used in GRAPES with SSI with additional views (a.iii) in the x−y plane prior to the sample and (a.iv) in the x−z plane at the sample for coincident pulses. (b) Different stages in data processing, including (b.i) the signal pulse 4 spatial spectral interferogram with the pulse 4 interferogram subtracted, (b.ii) the Fourier transform of (b.i) demonstrating peak shift/tilt due to a nonzero angle between pulses 3 and 4, and (b.iii) the pulse-tilt-corrected 2DFT spectrum. (Diagrams are not drawn to scale.)

prior to Fourier transformation. This process is multiplexed in GRAPES, where a range of τ delays are sampled simultaneously by tilting beam 1 relative to beam 2 and focusing with a cylindrical mirror to a line in the sample (Figure 1a.ii). Each point along the focal line in the sample has a unique τ value and is imaged onto a 2D image sensor in a spectrograph, yielding a set of τ-dependent interferograms for each laser shot.

In the work presented here, the wave vectors of beams 1, 2, and 3 and the signal ($\hat{\mathbf{k}}_1$, $\hat{\mathbf{k}}_2$, $\hat{\mathbf{k}}_3$, and $\hat{\mathbf{k}}_s$, respectively) form a rhombus (or diamond) at the crossing point in the sample (Figure 1a.ii and a.iii). Beams 1, 2, 3, and 4, initially parallel to one another, impinge on a GRAPES mirror, followed by a cylindrical concave mirror with its cylindrical axis aligned along x that focuses the beams to a line in the sample. The GRAPES mirror tilts beams 1 and 4 such that they cross beams 2 and 3 in the sample at a common focal line. Moving beam 1 further from beams 2 and 3 increases the crossing angle $\theta_{12} = \theta_1 - \theta_2$ in the sample (see Figure 1a.iv), thereby extending the range of sampled τ delays. Because beams 2 and 3 have a zero crossing angle in the x−z plane (see Figure 1a.iv), the time delay between pulses 2 and 3, or waiting time T, is constant along x.

When two plane wave electric fields ($\hat{\mathbf{E}}_i$ and $\hat{\mathbf{E}}_j$) of the form

$$\hat{\mathbf{E}}(\mathbf{r}, \omega) = e(\omega)\exp[i\phi(\omega) + i\hat{\mathbf{k}}(\omega)\cdot\mathbf{r}] \tag{1}$$

overlap spatially, their electric fields sum, yielding a spatiospectral intensity interference pattern given by

$$I(\mathbf{r}, \omega) \propto |\hat{\mathbf{E}}_i + \hat{\mathbf{E}}_j|^2 = |\hat{\mathbf{E}}_i|^2 + |\hat{\mathbf{E}}_j|^2 + \hat{\mathbf{E}}_i\hat{\mathbf{E}}_j^* + \hat{\mathbf{E}}_i^*\hat{\mathbf{E}}_j \tag{2}$$

where $|\hat{\mathbf{E}}_i|^2$ and $|\hat{\mathbf{E}}_j|^2$ are the intensity spectra of fields i and j, respectively, $e(\omega)$ is the spectral envelope, $\phi(\omega)$ is the spectral phase, $\hat{\mathbf{k}}(\omega)$ is the complex wave vector, and $\mathbf{r}$ is the position. (A circumflex or "hat" is used to denote complex-valued quantities, and bold face type is used for vectors.) The rightmost two terms in eq 2 contain the interference between the two fields. Using eq 1 to expand the $\hat{\mathbf{E}}_i\hat{\mathbf{E}}_j^*$ interference term yields

$$\hat{\mathbf{E}}_i(\mathbf{r}, \omega)\hat{\mathbf{E}}_j^*(\mathbf{r}, \omega) = e_i(\omega)e_j(\omega) \times \exp\{i[\phi_i(\omega) - \phi_j(\omega)] + i[\hat{\mathbf{k}}_i(\omega) - \hat{\mathbf{k}}_j(\omega)]\cdot\mathbf{r}\} \tag{3}$$

which contains the spectral phase difference $[\phi_i(\omega) - \phi_j(\omega)]$ and the spatiospectral interference wave vector $[\hat{\mathbf{k}}_i(\omega) - \hat{\mathbf{k}}_j(\omega)]$ between fields i and j.

For the typical case of propagation through a transparent medium (e.g., visible light in air), the imaginary part of the wave vector $\hat{\mathbf{k}}(\omega)$ is negligible such that $\hat{\mathbf{k}}(\omega) \approx \mathrm{Re}[\hat{\mathbf{k}}(\omega)] \equiv \mathbf{k}(\omega)$. Along the direction parallel to $[\mathbf{k}_i(\omega) - \mathbf{k}_j(\omega)]$ defined by a spatial detection unit vector $\mathbf{u}_{det}$, the spatial interference frequency is

$$k_{ij}^{int}(\omega) = \left\|\mathbf{k}_i(\omega) - \mathbf{k}_j(\omega)\right\| = 2\|\mathbf{k}(\omega)\|\sin\left(\frac{\theta_{ij}}{2}\right) \tag{4}$$

where $\|\hat{\mathbf{k}}(\omega)\| \equiv \|\hat{\mathbf{k}}_i(\omega)\| = \|\hat{\mathbf{k}}_j(\omega)\|$.

When using SSI, the GRAPES signal−reference interferogram (Figure 1b.i) is spatially modulated due to the spatially varying spectral phase difference between the signal and reference fields. The spatial dependence of the relative signal−reference spectral phase arises from the combination of two effects. First, a spatially varying τ, imprinted onto the sample by a nonzero tilt between pulses 1 and 2 [i.e., $\|\mathbf{k}_1(\omega) - \mathbf{k}_2(\omega)\| \neq 0$], results in a spatially varying signal spectral phase due to the inherent τ evolution of the third-order polarization in the sample; this is the phase that we ultimately want to retrieve. Second, a spatially varying signal−reference time delay is present at the detector due to a nonzero tilt between the signal and reference fields [i.e., $\|\mathbf{k}_s(\omega) - \mathbf{k}_4(\omega)\| \neq 0$]. In order to recover the τ-evolution of the signal relative to pulse 3, the signal−reference interferogram must be corrected to account

DOI: 10.1021/acs.jpclett.5b00273
J. Phys. Chem. Lett. 2015, 6, 945−950

for the tilt between pulses 3 and 4 because pulse 3 defines the zero of the spectral phase; this pulse tilt causes the peak shifts/tilts in Figure 1b.ii. First, to correct for variations in the spectrum and beam mode of the reference pulse, the signal−reference spatial spectral interferogram is divided by the square root of the spatial spectral interferogram containing only pulse 4. Second, the signal−reference spatial spectral interferogram is interpolated from an axis with equal wavelength steps onto an axis with equal frequency steps. The tilt correction is accomplished by multiplying the interpolated signal−reference spatial spectral interferogram $I_{s4}(\omega_t,x)$ (Figure 1b.i) by a complex-valued factor, yielding

$$\hat{I}^{c}_{s4}(\omega_t, x) = I_{s4}(\omega_t, x)\exp\{i[\mathbf{k}_4(\omega_t) - \mathbf{k}_3(\omega_t)]\cdot\mathbf{x}\} \quad (5)$$

where $[\mathbf{k}_4(\omega_t) - \mathbf{k}_3(\omega_t)]$ is extracted from spatial spectral interferograms between pulses 3 and 4 (see the Experimental Methods). Taking the fast Fourier transform of $\hat{I}^{c}_{s4}(\omega_t,x)$ along x yields the 2D signal $\hat{S}(\omega_t,\Delta k_x)$. Substituting for $k = \omega n/c$ gives the 2D signal spectrum $\hat{S}_{2D}(\omega_t,\omega_\tau)$ (Figure 1b.iii) as a function of the excitation frequency (ω_τ) and detection frequency (ω_t). This tilt correction procedure, which is valid for any signal−beam 4 crossing angle, is a generalization of the process used in prior GRAPES studies[12−14,25] that treated the special case of zero signal−beam 4 crossing angle. This procedure is robust to changes in optical alignment as long as the spatial spectral interferograms between beam pairs are acquired along with the signal interferograms under the same conditions.

2DFT spectra of Rb vapor and LH2 were measured using the GRAPES setup. Laser pulses with wavelengths spanning from 750 to 850 nm were generated through filamentation by focusing the output of a 1 kHz Ti:sapphire regenerative amplifier (Coherent, Legend Elite) into a pipe filled with 1 bar of argon, as previously described.[25] The output of the filamentation stage was compressed by a chirped mirror compressor and subsequently split using dielectric beam splitters into four beams, three excitation beams (for pulses 1, 2, and 3, each with 375 nJ pulse energy or $\sim 1.3 \times 10^{-4}$ J/cm^2 pulse fluence) and one reference beam (for pulse 4). The signal field was detected by SSI using a reference pulse (pulse 4) that propagates through the sample at an angle relative to the phase-matched signal direction $[\hat{\mathbf{k}}_s(\omega_t) \approx \hat{\mathbf{k}}_1(-\omega_1) + \hat{\mathbf{k}}_2(\omega_2) + \hat{\mathbf{k}}_3(\omega_3)]$, such that $\hat{\mathbf{k}}_4$ was rotated by $\sim 1°$ relative to $\hat{\mathbf{k}}_s$ toward $\hat{\mathbf{k}}_1$ (see Figure 1a.ii). SSI detection is simple to implement because modification of the crossing angle of the reference pulse relative to the signal field is the only alteration to the GRAPES apparatus that is necessary.

The collisionally broadened rubidium vapor D_1 ($5^2S_{1/2} \rightarrow 5^2P_{1/2}$, $\lambda_{eg} = 794.8nm$) and D_2 ($5^2S_{1/2} \rightarrow 5^2P_{3/2}$, $\lambda_{eg} = 780.0nm$) transitions are ideal candidates for detection by SSI since their peak shapes are exceptionally narrow ($\sim$0.3 cm^{-1} for 650 Torr of neon buffer gas) such that conventional FTSI with a spectrograph of typical resolution ($\delta\omega/2\pi c \approx 1$ cm^{-1}) would be unable to extract the spectral phase of the signal. In addition, the narrow peaks help demonstrate the frequency resolution and frequency accuracy of SSI. Both being coupled to a common ground state, the D_1 and D_2 transitions are expected to exhibit off-diagonal cross peaks due to excitation at one transition frequency producing signal at the other transition frequency.

The spatial spectral interferogram between the phase-matched 4WM signal from Rb vapor (at T = 1 ps) and the reference pulse shown in Figure 2 exhibits both high-frequency

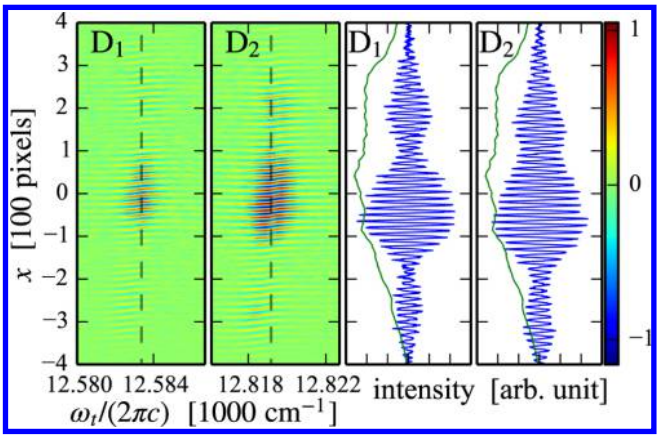

Figure 2. Spatial spectral interferogram of the 2DFT signal radiated by the D_1 transition (first panel) and the D_2 transition (second panel) interfering with pulse 4 as well as slices at the D_1 and D_2 central transition frequencies (indicated by dotted lines in the leftmost two panels) in the detection (ω_t) axis (rightmost two panels, blue lines). The beam 4 spatial profile along x is plotted for comparison (rightmost two panels, green lines). The 2DFT relaxation spectrum constructed from this spatial spectral interferogram is shown in Figure 3.

spatial modulation due to the nonzero signal−reference angle and low-frequency spatial modulation due to the beating between signals radiated at the D_1 and D_2 transition frequencies. In order to resolve the D lines from one another in the ω_τ dimension, the range of τ values sampled must be large enough to observe at least one period of their beat (difference) frequency $\tau_{D_2-D_1} = [(\omega_{eg}^{D_2} - \omega_{eg}^{D_1})/2\pi]^{-1} = 140$ fs in the spatial spectral interferogram, where $\omega_{eg}^{D_2}$ and $\omega_{eg}^{D_1}$ are the transition frequencies for the D_2 and D_1 lines, respectively. Beating between the D_1 and D_2 transitions is clearly visible in the slices taken from $\omega_t = \omega_{eg}^{D_1}$ and $\omega_t = \omega_{eg}^{D_2}$ in the rightmost two panes of Figure 2. While the total dephasing time of the collisionally broadened Rb D lines is on the order of 100 ps, the full extent of signal decay along τ is apodized by the finite transverse spatial mode of the beams. Because the τ range used here ($\sim$400 fs) was much smaller than the total dephasing time of the sample, along the ω_τ dimension, the shape and width of peaks in the measured 2DFT spectra are mostly determined by the beam transverse spatial profile and the sampled τ range, respectively.[26]

The absolute value 2DFT relaxation spectrum in Figure 3 contains D_1 and D_2 transition peaks along the diagonal ($\omega_\tau = -\omega_t$) and two cross peaks indicating coupling between the D_1 and D_2 transitions. As stated above, the peak shapes and widths along the ω_τ dimension are merely reflective of the excitation frequency resolution function of the experimental apparatus. However, this is not a fundamental limitation because the ω_τ resolution can be increased to match the ω_t resolution by increasing the experimentally sampled τ range, as is planned for future work. Along the ω_t dimension, the expected D transition line widths are on the order of the resolution of the spectrograph. The peaks at $\omega_t = \omega_{eg}^{D_2}$ exhibit slight splitting that can be attributed to absorptive propagation distortions[24,27] wherein the radiated 4WM signal is reabsorbed by the sample.[10]

A constant offset ($\sim$270 cm^{-1}) in the D line peak positions is present in the excitation frequency (ω_τ) axis compared to the detection frequency (ω_t) axis. While the accuracy of both

DOI: 10.1021/acs.jpclett.5b00273
J. Phys. Chem. Lett. 2015, 6, 945−950

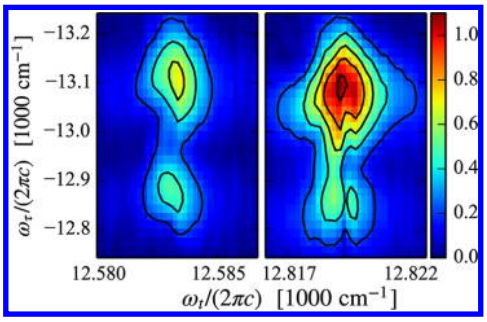

Figure 3. Absolute value 2DFT relaxation spectrum of the D_1 and D_2 transitions of Rb vapor in Ne buffer gas at T = 1ps. The signal detected at the D_1 (D_2) transition frequency is shown in the left (right) pane. The axis scales have been adjusted to show similar peak widths in each dimension and an axis break introduced between the D_1 and D_2 transitions in the detection axis.

frequency axes is limited by the calibration accuracy of the spectrograph, the excitation axis is also limited in accuracy by two additional effects, (1) the accuracy of $\Delta\tau_{12}(x)$ values derived from the spatial spectral interferogram between pulses 1 and 2 and used to determine the τ axis and (2) the accuracy of the tilt correction factor in eq 5 derived from the spatial spectral interferogram between pulses 3 and 4.

LH2 has two main absorption bands in the near-infrared, B800 (λ_{eg} = 799 nm) and B850 (λ_{eg} = 847 nm). These spectrally broad ($\delta\lambda$ > 40 nm) bands are coupled, resulting in cross peaks that evolve in T as the system relaxes. The intense above-diagonal cross peak arises from energy transfer, while the faint below-diagonal cross peak appears due to band coupling.[13]

An absolute value "rephasing-like" (see the Experimental Methods) 2DFT spectrum of LH2 at a waiting time of 1000 fs is shown in Figure 4. Initially at T = 0, diagonal peaks at $\omega_t/2\pi c$

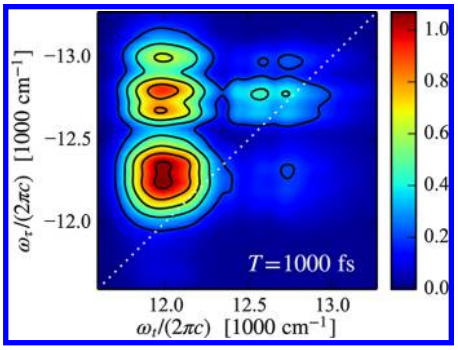

Figure 4. Absolute value 2DFT rephasing-like spectrum of LH2 at T = 1000 fs, smoothed along ω_t to match the frequency resolution of ω_τ.

= 12000 and 12750 cm^{-1} are present, attributed to the B850 and B800 bands, respectively. By T = 1000 fs (Figure 4), the diagonal B800 peak has diminished, transferring amplitude into an above-diagonal cross peak shared between the B800 and B850 bands. (The structure in the higher-frequency peak(s) is a consequence of structure in the spectrum and beam mode of the excitation and reference pulses.) This above-diagonal cross peak contains signal radiated by the B850 band arising from excitation of the B800 band and grows as a function of waiting time, indicating that a population of chromophores initially excited to the B800 state relax to the B850 state on a ∼1 ps time scale. By T = 2000 fs, the B800 diagonal peak is almost completely gone, leaving only two features in the 2DFT spectrum, the B850 diagonal peak and the above-diagonal cross peak.

In order to empirically compare the results of SSI and FTSI, an additional set of 2DFT spectra of LH2 was collected under identical experimental conditions except that a time delay between pulses 3 and 4 was introduced and the spectrograph entrance slit was narrowed to increase spectral resolution. The resulting data were processed using the FTSI method as in previous work.[12,25,28] Compared to SSI, a narrower slit is necessary with FTSI in order to sufficiently resolve the sharp spectral interference fringes induced by a time delay between pulses 3 and 4. Decreasing the slit width causes a corresponding reduction in the throughput of the spectrograph, ultimately leading to lower signal detection efficiency. In our case, the integrated intensity from one camera exposure of the signal−pulse 4 interferogram (after subtraction of the pulse 4 interferogram) was more than 2.5 times greater with SSI than that with FTSI.

Slight variations in the time delay between pulses 1 and 2 as well as pulses 3 and 4 (due to mechanical vibrations of the experimental apparatus, air currents, etc.) cause interference fringes to shift spatially on the detector over time. Because partial cancellation occurs when summing multiple camera exposures with shifted interference fringes, fringe amplitude does not linearly increase with the number of camera exposures summed, reducing the effectiveness of signal averaging. Such losses in averaging are more severe for FTSI than SSI in our experiment, likely due to the higher spatial frequency of spectral fringes present at the detector in FTSI. For a typical data set containing 100 camera exposures, these differences amount to a factor of ∼5 improvement in signal collection efficiency for SSI compared to FTSI.

The 2DFT spectra of LH2 produced by SSI and FTSI are qualitatively identical. Peak shapes and widths are visually indistinguishable at the full range of measured waiting times (T = 0−2000 fs), and the same relaxation dynamics are observed when using both methods.

In conclusion, we have demonstrated the recovery of 4WM signals using SSI. SSI is a generalized approach to interferometry that exploits both the spatial and spectral properties of light to fully characterize its spectrum and phase. We applied the SSI method to measuring 2DFT spectra of Rb vapor and LH2 protein, which exhibit drastically different line widths. SSI improves the frequency resolution of spectral phase recovery compared to conventional FTSI methods, enabling the full frequency resolution of the spectrograph to be utilized and thus improving the ability to study chromophores with narrow spectral features. Combining spatial interferometry with spectral interferometry introduces additional methods for isolating the signal from DC contaminants, thereby increasing the sensitivity of 4WM measurements. In addition, SSI enables more efficient and sensitive signal detection by alleviating the need to resolve high-frequency spectral interference patterns. Best of all, these improvements in frequency resolution and sensitivity compared to FTSI GRAPES are achieved without any additional experimental complexity.

EXPERIMENTAL METHODS

Pulse Timing and Tilt Characterization. The relative spectral phases and spatiospectral interference wave vectors between pulses 1, 2, 3, and 4 are extracted from spatial spectral interferograms between pairs of pulses using a Fourier transform method. Starting from a spatial spectral interfero-

DOI: 10.1021/acs.jpclett.5b00273
J. Phys. Chem. Lett. 2015, 6, 945−950

gram $[I_{ij}(\lambda_t,x)]$ between pulses i and j containing the light intensity as a function of a spectral dimension (λ_t) and an orthogonal spatial dimension (x), the interferogram is interpolated along λ_t onto an axis of equally spaced frequency points (ω_t). The resulting interpolated interferogram is fast Fourier transformed (FFT) along both ω_t and x axes to produce $I_{ij}(t,\Delta k_x)$. As long as each pair of beams has a relative time delay, a relative wavefront tilt along the x axis, or both, $I_{ij}(t,\Delta k_x)$ can be filtered to eliminate the DC peak [centered at $I_{ij}(t = 0,\Delta k_x = 0]$, leaving only the AC interference peaks. The filtered data is then inverse FFT along both dimensions to give the filtered, interpolated interferogram $I^f_{ij}(\omega_t,x)$.

$I^f_{ij}(\omega_t,x)$ is FFT along x, yielding $I^f_{ij}(\omega_t,\Delta k_x)$. For beams that cross entirely in the plane normal to x, no spatial interference is formed along x, resulting in only a DC peak at $\Delta k_x = 0$. Otherwise, two AC peaks are observed at $\Delta k_x = \pm k_{ij}^{\text{int}}$ (related by reflection symmetry about the line $\Delta k_x = 0$). For beams with spatiotemporal profiles differing only in their angles relative to the x axis, the AC peaks are tilted due to the frequency dependence of the wave vector k_{ij}^{int}, lying along the lines

$$\Delta k_x(\omega_t) = \pm k_{ij}^{\text{int}}(\omega_t) = \pm 2\frac{\omega_t n}{c}\sin\left(\frac{\theta_{ij}}{2}\right) \tag{6}$$

where θ_{ij} is the angle between the beams i and j forming the interferogram. The recovered θ_{ij} [or, equivalently, $k_{ij}^{\text{int}}(\omega_t)$] is used in signal isolation and processing to compensate for the signal−beam 4 angle.

The filtered, interpolated interogram $[I^f_{ij}(\omega_t,x)]$ is FFT along ω_t, yielding $I^f_{ij}(t,x)$. This contains the spatiotemporal cross correlation between pulses i and j with peaks lying along $t = \pm\Delta\tau_{ij}(x) = \pm\sin(\theta_{ij})xn/c$, where $\Delta\tau_{ij}(x)$ is the relative time delay between pulses i and j. The recovered $\Delta\tau_{12}(x)$ for beams 1 and 2 is used to generate the τ and ω_τ axes. Similarly, $\Delta\tau_{23}(x)$ for beams 2 and 3 determines the waiting time T, which has no x dependence in this beam geometry due to the zero crossing angle (relative to the x axis) between beams 2 and 3.

Rubidium Vapor Sample. A 22 mm diameter, 1 mm path length quartz sample cell containing a small amount of solid rubidium metal and filled with 650 Torr of neon buffer gas at 24 °C (Triad Technology) was heated to 120 °C, increasing the vapor pressure[29] of Rb to ∼0.84 mTorr. The neon buffer gas collisionally broadened the Rb D_1 and D_2 lines to the point that the hyperfine structure was unresolved. On the basis of the temperature and partial pressures of gases in the sample cell, the peak absorbance of the D_2 transition was calculated to be ∼3.7.

LH2 Sample. LH2 in a pH 8 TRIS buffer solution was circulated by a peristaltic pump through a 250 μm path length flow cell. The peak absorbances of the B800 and B850 bands were 0.27 and 0.43, respectively. 2DFT "rephasing-like" spectra were collected at waiting times ranging from $T = 0$ to 2000 fs. The 2DFT spectra are described as rephasing-like because the introduction of a small (∼200 fs) delay between pulses 1 and 2 causes positive (rephasing) τ delays to be more heavily weighted than negative (nonrephasing) τ delays, approximating a 2DFT rephasing spectrum in which only positive τ delays are sampled.

AUTHOR INFORMATION

Corresponding Author

*E-mail: elharel@northwestern.edu.

Notes

The authors declare no competing financial interest.

ACKNOWLEDGMENTS

We thank P. Dahlberg and G. S. Engel for generously providing us with LH2 samples. This work was supported by the Army Research Office (W911NF-13-1-0290), the Air Force Office of Scientific Research (FA9550-14-1-0005), and the Packard Foundation (2013-39272) in part.

REFERENCES

(1) Hybl, J. D.; Albrecht, A. W.; Gallagher Faeder, S. M.; Jonas, D. M. Two-Dimensional Electronic Spectroscopy. *Chem. Phys. Lett.* **1998**, *297*, 307−313.

(2) Zhang, W. M.; Chernyak, V.; Mukamel, S. Multidimensional Femtosecond Correlation Spectroscopies of Electronic and Vibrational Excitons. *J. Chem. Phys.* **1999**, *110*, 5011−5028.

(3) Hybl, J. D.; Albrecht Ferro, A.; Jonas, D. M. Two-Dimensional Fourier Transform Electronic Spectroscopy. *J. Chem. Phys.* **2001**, *115*, 6606−6622.

(4) Jonas, D. M. Two-Dimensional Femtosecond Spectroscopy. *Annu. Rev. Phys. Chem.* **2003**, *54*, 425−463.

(5) Khalil, M.; Demirdöven, N.; Tokmakoff, A. Coherent 2D IR Spectroscopy: Molecular Structure and Dynamics in Solution. *J. Phys. Chem. A* **2003**, *107*, 5258−5279.

(6) West, B. A.; Moran, A. M. Two-Dimensional Electronic Spectroscopy in the Ultraviolet Wavelength Range. *J. Phys. Chem. Lett.* **2012**, *3*, 2575−2581.

(7) Cundiff, S. T.; Zhang, T.; Bristow, A. D.; Karaiskaj, D.; Dai, X. Optical Two-Dimensional Fourier Transform Spectroscopy of Semiconductor Quantum Wells. *Acc. Chem. Res.* **2009**, *42*, 1423−1432.

(8) Harel, E.; Rupich, S. M.; Schaller, R. D.; Talapin, D. V.; Engel, G. S. Measurement of Electronic Splitting in PbS Quantum Dots by Two-Dimensional Nonlinear Spectroscopy. *Phys. Rev. B* **2012**, *86*, 075412.

(9) Dai, X.; Bristow, A. D.; Karaiskaj, D.; Cundiff, S. T. Two-Dimensional Fourier-Transform Spectroscopy of Potassium Vapor. *Phys. Rev. A* **2010**, *82*, 052503.

(10) Li, H.; Spencer, A. P.; Kortyna, A.; Moody, G.; Jonas, D. M.; Cundiff, S. T. Pulse Propagation Effects in Optical 2D Fourier-Transform Spectroscopy: Experiment. *J. Phys. Chem. A* **2013**, *117*, 6279−6287.

(11) Fecko, C. J.; Eaves, J. D.; Loparo, J. J.; Tokmakoff, A.; Geissler, P. L. Ultrafast Hydrogen-Bond Dynamics in the Infrared Spectroscopy of Water. *Science* **2003**, *301*, 1698−1702.

(12) Harel, E.; Long, P. D.; Engel, G. S. Single-Shot Ultrabroadband Two-Dimensional Electronic Spectroscopy of the Light-Harvesting Complex LH2. *Opt. Lett.* **2011**, *36*, 1665−1667.

(13) Harel, E.; Engel, G. S. Quantum Coherence Spectroscopy Reveals Complex Dynamics in Bacterial Light-Harvesting Complex 2 (LH2). *Proc. Natl. Acad. Sci. U.S.A.* **2012**, *109*, 706−711.

(14) Harel, E.; Fidler, A. F.; Engel, G. S. Real-Time Mapping of Electronic Structure with Single-Shot Two-Dimensional Electronic Spectroscopy. *Proc. Natl. Acad. Sci. U.S.A.* **2010**, *107*, 16444−16447.

(15) Lepetit, L.; Chériaux, G.; Joffre, M. Linear Techniques of Phase Measurement by Femtosecond Spectral Interferometry for Applications in Spectroscopy. *J. Opt. Soc. Am. B* **1995**, *12*, 2467−2474.

(16) Fittinghoff, D. N.; Walmsley, I. A.; Bowie, J. L.; Sweetser, J. N.; Jennings, R. T.; Krumbügel, M. A.; DeLong, K. W.; Trebino, R. Measurement of the Intensity and Phase of Ultraweak, Ultrashort Laser Pulses. *Opt. Lett.* **1996**, *21*, 884−886.

(17) Fittinghoff, D. N.; Bowie, J. L.; Sweetser, J. N.; Jennings, R. T.; Krumbügel, M. A.; DeLong, K. W.; Trebino, R.; Walmsley, I. A. Measurement of the Intensity and Phase of Ultraweak, Ultrashort Laser Pulses: Erratum. *Opt. Lett.* **1996**, *21*, 1313.

(18) Gallagher, S. M.; Albrecht, A. W.; Hybl, J. D.; Landin, B. L.; Rajaram, B.; Jonas, D. M. Heterodyne Detection of the Complete Electric Field of Femtosecond Four-Wave Mixing Signals. *J. Opt. Soc. Am. B* **1998**, *15*, 2338−2345.

DOI: 10.1021/acs.jpclett.5b00273
J. Phys. Chem. Lett. 2015, 6, 945−950

(19) Albrecht, A. W.; Hybl, J. D.; Gallagher Faeder, S. M.; Jonas, D. M. Experimental Distinction Between Phase Shifts and Time Delays: Implications for Femtosecond Spectroscopy and Coherent Control of Chemical Reactions. *J. Chem. Phys.* **1999**, *111*, 10934.
(20) Gallagher Faeder, S. M.; Jonas, D. M. Phase-Resolved Time-Domain Nonlinear Optical Signals. *Phys. Rev. A* **2000**, *62*, 033820.
(21) Bowlan, P.; Gabolde, P.; Shreenath, A.; McGresham, K.; Trebino, R.; Akturk, S. Crossed-Beam Spectral Interferometry: A Simple, High-Spectral-Resolution Method for Completely Characterizing Complex Ultrashort Pulses in Real Time. *Opt. Express* **2006**, *14*, 11892−11900.
(22) Tanabe, T.; Tanabe, H.; Teramura, Y.; Kannari, F. Spatiotemporal Measurements Based on Spatial Spectral Interferometry for Ultrashort Optical Pulses Shaped by a Fourier Pulse Shaper. *J. Opt. Soc. Am. B* **2002**, *19*, 2795−2802.
(23) Gallagher Faeder, S. M.; Jonas, D. M. Two-Dimensional Electronic Correlation and Relaxation Spectra: Theory and Model Calculations. *J. Phys. Chem. A* **1999**, *103*, 10489−10505.
(24) Belabas, N.; Jonas, D. M. Three-Dimensional View of Signal Propagation in Femtosecond Four-Wave Mixing with Application to the Boxcars Geometry. *J. Opt. Soc. Am. B* **2005**, *22*, 655−674.
(25) Spokoyny, B.; Harel, E. Mapping the Vibronic Structure of a Molecule by Few-Cycle Continuum Two-Dimensional Spectroscopy in a Single Pulse. *J. Phys. Chem. Lett.* **2014**, 2808−2814.
(26) By the Fourier convolution theorem, the measured peak shape in the ω_τ dimension is the convolution of the spectrum of the induced polarization with the Fourier transform of the beam transverse spatial mode (as a function of τ).
(27) Yetzbacher, M. K.; Belabas, N.; Kitney, K. A.; Jonas, D. M. Propagation, Beam Geometry, and Detection Distortions of Peak Shapes in Two-Dimensional Fourier Transform Spectra. *J. Chem. Phys.* **2007**, *126*, 044511.
(28) Harel, E.; Fidler, A. F.; Engel, G. S. Single-Shot Gradient-Assisted Photon Echo Electronic Spectroscopy. *J. Phys. Chem. A* **2011**, *115*, 3787−3796.
(29) Alcock, C. B.; Itkin, V. P.; Horrigan, M. K. Vapour Pressure Equations for the Metallic Elements: 298−2500 K. *Can. Metall. Q.* **1984**, *23*, 309−313.

DOI: 10.1021/acs.jpclett.5b00273
J. Phys. Chem. Lett. 2015, 6, 945−950